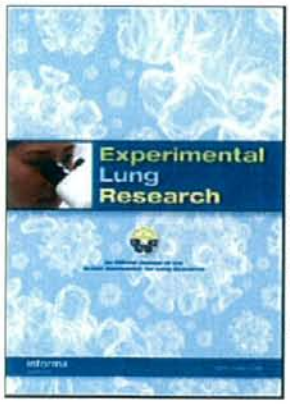

Experimental Lung Research
Publication details, including instructions for authors and subscription information:
http://www.informaworld.com/smpp/title~content=t713722902

C-REACTIVE PROTEIN MODULATES HUMAN LUNG FIBROBLAST MIGRATION

Kazuhiko Kikuchi [a]; Tadashi Kohyama [a]; Yasuhiro Yamauchi [a]; Jun Kato [a]; Kazutaka Takami [a]; Hitoshi Okazaki [b]; Masashi Desaki [a]; Takahide Nagase [a]; Stephen I. Rennard [c]; Hajime Takizawa [d]
[a] Department of Respiratory Medicine, University of Tokyo, Tokyo, Japan [b] Research and Development Department, Central Blood Institute, Blood Service Headquarters, Japanese Red Cross Society, Tokyo, Japan [c] Pulmonary and Critical Care Medicine Section, University of Nebraska Medical Center, Omaha, Nebraska, USA [d] Fourth Department of Internal Medicine, Teikyo University, Tokyo, Japan

Online Publication Date: 01 February 2009

To cite this Article Kikuchi, Kazuhiko, Kohyama, Tadashi, Yamauchi, Yasuhiro, Kato, Jun, Takami, Kazutaka, Okazaki, Hitoshi, Desaki, Masashi, Nagase, Takahide, Rennard, Stephen I. and Takizawa, Hajime(2009)'C-REACTIVE PROTEIN MODULATES HUMAN LUNG FIBROBLAST MIGRATION',Experimental Lung Research,35:1,48 — 58

To link to this Article: DOI: 10.1080/01902140802404138

URL: http://dx.doi.org/10.1080/01902140802404138

Experimental Lung Research, 35:48–58, 2009

ISSN: 0190-2148 print / 1521-0499 online
DOI: 10.1080/01902140802404138

informa
healthcare

C-REACTIVE PROTEIN MODULATES HUMAN LUNG FIBROBLAST MIGRATION

Kazuhiko Kikuchi, Tadashi Kohyama, Yasuhiro Yamauchi, Jun Kato, and Kazutaka Takami ☐ *Department of Respiratory Medicine, University of Tokyo, Tokyo, Japan*

Hitoshi Okazaki ☐ *Research and Development Department, Central Blood Institute, Blood Service Headquarters, Japanese Red Cross Society, Tokyo, Japan*

Masashi Desaki and Takahide Nagase ☐ *Department of Respiratory Medicine, University of Tokyo, Tokyo, Japan*

Stephen I. Rennard ☐ *Pulmonary and Critical Care Medicine Section, University of Nebraska Medical Center, Omaha, Nebraska, USA*

Hajime Takizawa ☐ *Fourth Department of Internal Medicine, Teikyo University, Tokyo, Japan*

☐ *C-reactive protein (CRP) has been classically used as a marker of inflammation. The aim of this study was to investigate the effect of CRP on migration of human fetal lung fibroblasts (HFL-1) to human plasma fibronectin (HFn). Using the blindwell chamber technique, CRP inhibited HFL-1 migration in a dose-dependent fashion (at 1 μg/mL, inhibition: 32.5% ± 7.1%; $P < .05$). Western blot analysis showed that CRP inhibited the p38 mitogen-activated protein kinase (MAPK) activity in the presence of HFn. Moreover, the MAPK inhibitors SB202190 (25 μM) and SB203580 (25 μM) inhibited HFn-induced cell migration, suggesting an important role of p38 MAPK in HFn-induced migration. Taken together, these results suggest that the inhibitory effect of CRP is mediated by blocking MAPK. In summary, this study demonstrates that CRP directly modulates human lung fibroblasts migration. Thus, CRP may contribute to regulation of wound healing and may be endogenous antifibrotic factor acting on lung fibrosis.*

Keywords lung fibroblast, C-reactive protein MAPK, migration

Idiopathic pulmonary fibrosis is characterized by excess accumulation of fibroblasts and extracellular matrix in the lung parenchyma. Although it

Received 3 April 2008; accepted 11 August 2008.
The authors thank Miss Makiko Kase for her excellent technical assistance.
Address correspondence to Tadashi Kohyama, MD, PhD, School of Medicine, Tokyo University, 7-3-1 Hongo Bunkyo-ku, Tokyo, Japan. E-mail: koyama-tky@umin.ac.jp

has been believed that alveolitis, alveolar wall inflammation, is the central pathogenic mechanism for the development of pulmonary fibrosis, conventional anti-inflammatory therapy does not improve this disorder. Thus, it is necessary to find new therapeutic strategies for this intractable disease.

C-reactive protein (CRP) is one of the acute-phase proteins that is mostly derived from the liver. It has a molecular weight of 105 kDa, and is induced by inflammatory stimuli, usually in association with increased neutrophils in the peripheral blood. It has been established that CRP is a useful serum marker for evaluation of disease activity and therapeutic response in a variety of conditions, including bacterial infection [1], myocardial infarction [2], and acute respiratory distress syndrome [3, 4].

Recent studies have shown that CRP is not only an acute-phase reactant but also is a modulator of inflammation [4]. CRP inhibits neutrophil chemotaxis through p38 mitogen-activated protein kinase (MAPK) inhibition [5, 6], attenuates nitric oxide production by endothelial cells [7], and up-regulates angiotensin type 1 receptors in vascular smooth muscle [8]

It has recently been demonstrated that CRP is localized in bronchial airways [9]. Moreover, Arase and associates showed that serum levels of CRP are increased prior to the onset of idiopathic pulmonary fibrosis [10]. These findings raise the possibility that CRP may play some roles in the pathogenesis of idiopathic pulmonary fibrosis, although the actual role of CRP in the lung remains unknown.

The current study was designed to explore the hypothesis that CRP could modulate lung fibroblast migration and could contribute to the fibrotic process in the lung.

MATERIALS AND METHODS

Materials

One of the recombinant CRPs expressed in *Escherichia coli*, SB202190, and SB203580 were purchased from Calbiochem (La Jolla, CA). This recombinant CRP was provided by liquid form (1 mg/mL), which contained 140 mM NaCl, 20 mM Tris-HCl, 2 mM $CaCl_2$, and 0.05% NaN_3. Then we used 0.005% NaN_3as solvent control, which was the same concentration of 100 μg/mL CRP solution (see Figures 2, 5). Another recombinant CRP, which is expressed in the mouse myeloma cell line NS0 and is free from sodium azide and endotoxin, was purchased from R&D Systems (Minneapolis, MN). The azide- and endotoxin-free (<1.0 EU per 1 μg) CRP was dissolved into 0.1% bovine serum albumin–containing phosphate buffered saline (PBS) as a 10 μg/mL of stock solution. As this CRP solution contained 20 mM Tris, 0.2 M NaCl, 5 mM $CaCl_2$, we adjusted the concentration of solvent control to 100 μg/mL CRP (Figure 2) or 10 μg/mL CRP (Figure 3). In this

article, CRP that was free from endotoxin and azide is referred as azide- or endotoxin-free CRP and CRP not free from azide and endotoxin is referred as conventional CRP. SB202190 (25 mM) and SB203580 (25 mM) were dissolved in DMSO and diluted in medium before use. The human plasma fibronectin and lipopolysaccharide (LPS) were purchased from Sigma (St. Louis, MO). LPS was dissolved into saline as stock solution. Tissue culture supplements and media were purchased from Gibco (Life Technologies, Grand Island, NY). Fetal calf serum (FCS) was purchased from Biofluid (Rockville, MD).

Cell Cultures

Human fetal lung fibroblasts (HFL-1) were purchased from the American Type Culture Collection (Rockville, MD). The cells were cultured in 100-mm tissue culture dishes (IWAKI; Japan) in Ham's F12 medium (F12; Sigma), and supplemented with 10% fetal calf serum (FCS; Biofluid), 50 U/mL penicillin, and 50 μg/mL streptomycin in a 37°C, 5% CO_2 incubator. Subconfluent fibroblasts were trypsinized (0.05% trypsin EDTA solution; Gibco) in order to passage cells. All experiments were conducted between the 9th and 20th passages.

Chemotaxis Assay

Cell migration of HFL-1 was assessed by the modified Boyden blindwell chamber technique [11] using a 48-well chamber (Nucleopore, Cabin John, MD) as previously reported [12]. In general, 50 μL of fetal lung fibroblasts in serum-free F12 (1.0×10^6/mL) were placed in the top wells of the chamber with the desired concentrations of CRP or other reagents. For investigation of priming, HFL-1 cells were preincubated on the culture dishes with the desired concentrations of reagents for 30 minutes in F12 without serum, following which they were trypsinized and used for the migration assay. The chemoattractant (20 μg/mL of HFn) was placed in the bottom chamber. The 2 wells were separated by an 8-μm-pore filter (Nucleopore, Pleasanton, CA) coated with 0.1% gelatin (Bio-Rad, Hercules, CA). The chamber was incubated at 37°C in a moist, 5% CO_2 atmosphere. Except as indicated, chambers were incubated for 6 hours, after which the cells above the filter were removed by scraping. The filter was then fixed, stained with Diff Quik stain (International reagents, Kobe, Japan), and mounted on a glass microscope slide. Migration was assessed by counting the number of cells in 5 randomly selected high-power fields using a light microscope. Triplicate wells were prepared in each experiment for every condition. At least 3 separate experiments were performed with different cell cultures of HFL-1.

Western Blot Analysis

The p38 MAPK activity was determined by using Western blot analysis. After growth to subconfluence in 6-well plates (Becton Dickinson, Franklin Lakes, NJ, USA), HFL-1 cells were washed with PBS 2 times. The cells were then treated with or without various concentrations of CRP with 20 μg/mL of HFn. Because the CRP solutions contained sodium azide, in order to exclude an effect of the solvent, the same concentrations of sodium azide alone were also added in separate cultures without CRP. After 10 minutes' incubation, the cells were solubilized with 250 μL of 2× sodium dodecyl sulfate–polyacrylamide gel electrophoresis (SDS-PAGE) sample buffer (125 mM Tris-HCl [pH 6.8], 4.6% SDS, 20% glycerol, 10% 2 ME [2-mercaptoethanol], BPB [bromo phenol blue]). The samples were heated in a boiled water bath for 5 minutes to denature the proteins and centrifuged at 12000 revolutions per minute for 10 minutes to remove the debris. The sample protein was separated in a 10% polyacrylamide gel and transferred onto Transfer Membranes (Millipore, Bedford, MA). Each membrane was stained with Ponceau S (Sigma) for protein to verify equal loading and transfer. Membranes were blocked with 3% bovine serum albumin (Sigma) in Tris-buffered saline with 0.1% Tween 20 (Sigma) for 1 hour. Membrane were then reacted with specific antibodies (Cell Signaling Technology, Danvers, MA) against p38 MAPK or phosphorylated p38 MAPK, followed by incubation with horseradish peroxidase (HRP)-conjugated anti-rabbit second antibody (Cell Signaling Technology). The results were visualized by chemiluminescence using enhanced chemiluminescence (ECL) (Amersham Biosciences, Piscataway, NJ) according to the manufacturer's instructions. ECL is a light-emitting nonradioactive method for detection of immobilized specific antigens with HRP-labeled antibodies, as reported previously [13].

Statistical Analysis

Results were confirmed by repeating experiments on at least 3 separate occasions, each performed in triplicate. Data shown in figures were pooled data for all experiments expressed as mean ± SEM. Samples with multiple comparisons were analyzed for significance using analysis of variance (ANOVA). Where ANOVA indicated significant differences between groups, the Fisher's exact probability test was applied and $P < .05$ was considered as significant.

RESULTS

Because one of the recombinant CRP we used was not free from endotoxin, we checked whether lung fibroblast migration was influenced by LPS, which is known as endotoxin. LPS had no effect on lung fibroblast

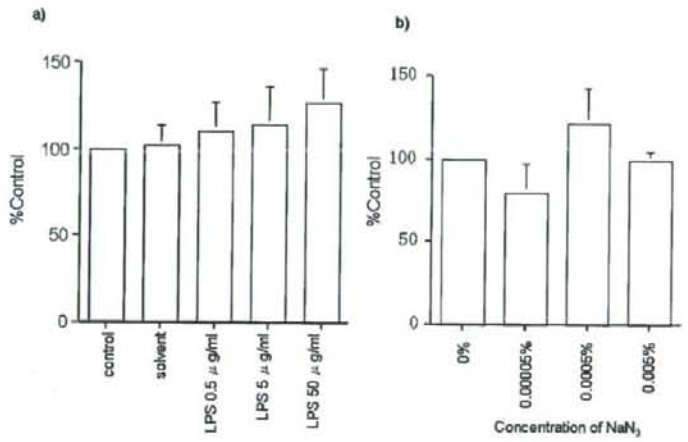

FIGURE 1 The effect of LPS or sodium azide on HFL-1 migration. CRP effect, which was known as endotoxin or sodium azide on HFL-1 migration, were assayed with the Boyden blindwell chamber assay system. HFn (20 μg/mL) was used as the chemoattractant. LPS (*a*) or sodium azide (*b*) at various concentrations were added to the fibroblasts in the top wells of the chemotaxis chamber. Vertical axis: fibroblast migration expressed as percentage of that of control. Horizontal axis: (*a*) LPS (μg/ml); solvent: saline. (*b*) Sodium azide: 0.00005%, 0.0005%, and 0.005% indicate concentration of NaN_3 of 1, 10, and 100 μg/mL CRP solution, respectively. Data are presented as the mean + SEM from 3 separate experiments, each studied in triplicate cultures.

migration (Figure 1*a*). As there is also the possibility that the effects of commercial CRP are caused by biologically active contaminants such as sodium azide [14, 15], we studied the sodium azide effect on lung fibroblast migration. We put the same concentration of sodium azide without CRP (1 μg/mL of CRP contained 0.00005% NaN_3). There was no significant difference between control and other concentrations of NaN_3 we checked (Figure 1*b*).

Fibronectin led HFL-1 in a concentration-dependent manner as previously reported [16]. In the presence of 20 μg/mL HFn, the number of migrated HFL-1 reached to 175 $\pm$ 28.8 ($n = 5$). We used fibronectin as chemoattractant for HFL-1. Both CRPs (1 to 100 μg/mL) added to the upper wells together with the fibroblasts inhibited the migration. CRP consistently inhibited HFL-1 migration at concentrations ranging between 0 and 100 μg/mL (azide- and endotoxin-free CRP: 32.5% $\pm$ 7.1% inhibition at 1 μg/mL, $P < .05$; conventional CRP: 21.3% $\pm$ 2.5% inhibition at 1 μg/mL, $P < .05$) (Figure 2). Time course studies demonstrated that the number of fibroblasts that accumulated on the bottom side of the membrane was significantly inhibited by 10 μg/mL of azide- and endotoxin-free CRP when incubation periods were over 6 hours (Figure 3).

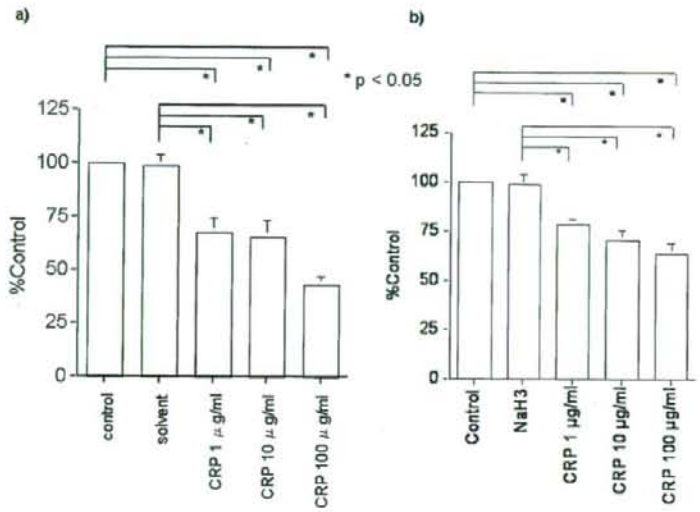

FIGURE 2 Concentration-dependent inhibition of fibroblast migration by azide- and endotoxin-free CRP (*a*) and conventional CRP (*b*). Migration of HFL-1 was assayed with the Boyden blindwell chamber assay system. HFn (20 μg/mL) was used as the chemoattractant. The azide- or endotoxin-free CRP at various concentrations was added to the fibroblasts in the top wells of the chemotaxis chamber. Vertical axis: fibroblast migration expressed as percentage of that of control. Horizontal axis: CRP concentration (μg/mL). NaN_3: 0.005% sodium azide solvent for conventional CRP. Data are presented as the mean + SEM from 3 separate experiments, each studied in triplicate cultures. $^*P < .05$

Because there is a report that shows that neutrophil migration driven by fMLP is mediated by the p38 MAPK pathway, we next tried to determine if the fibroblast migration driven by HFn is also mediated by the p38 MAPK pathway and if the CRP effect is related to this mechanism. To accomplish this, we examined the effect of the specific p38 MAPK inhibitors SB203580 or SB202190 on HFn-mediated migration. Both inhibitors inhibited fibroblast migration to HFn to a degree similar to that observed with CRP (Figure 4*a, b*). In addition, we examined the activation of p38 MAPK by Western blot analysis. Sodium azide, at the concentrations used, had no effect on p38 MAPK activity. In the current studies, 20 μg/mL of HFn for 10 minutes' incubation was used according to preliminary evaluation. As shown in Figure 5, CRP inhibited the phosphorylated p38 MAPK in the presence of HFn (Figure 5).

DISCUSSION

In this report, we showed that CRP was capable of inhibiting lung fibroblast migration to human fibronectin in a concentration-dependent fashion

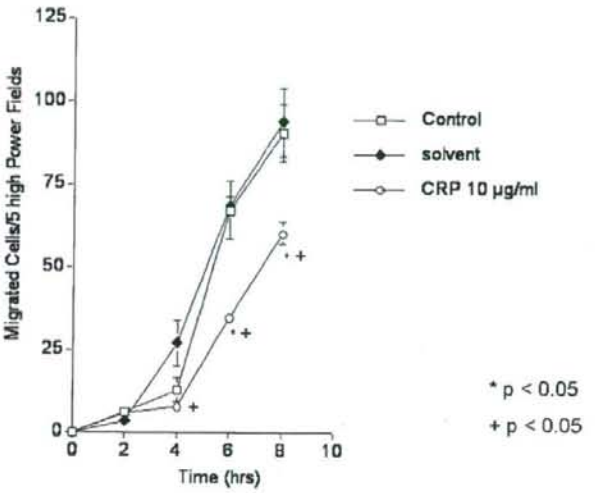

FIGURE 3 Time course effect of azide- and endotoxin-free CRP on HFn-induced fibroblast migration. Migration of HFL-1 was assayed with the Boyden blindwell chamber assay system. HFn (20 μg/mL) was used as chemoattractant. The azide- and endotoxin-free CRP was added to the fibroblasts in the top wells at 10 μg/mL. Solvent: solvent for azide- and endotoxin-free CRP. Vertical axis: fibroblast migration expressed as number of cells migrated per 5 high-power fields; horizontal axis: incubation time in hours. The data are from a single experiment representative of triplicate assays. Data are presented as the mean ± SEM from triplicate wells. *, compared with control; +, compared with solvent.

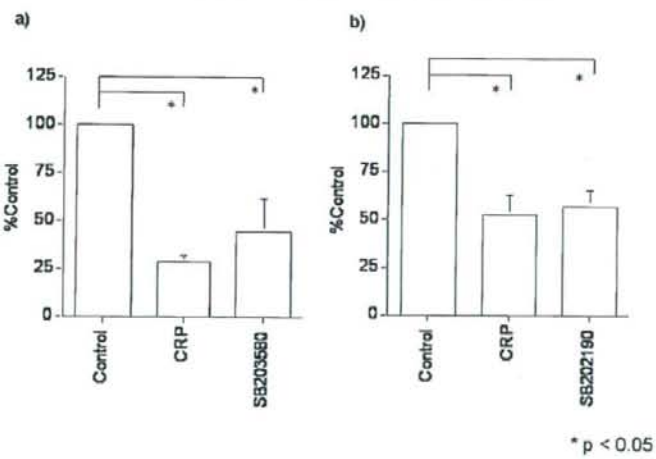

FIGURE 4 Effect of the MAPK inhibitors and CRP on inhibition of fibroblast migration. MAPK inhibitors or CRP (10 μg/mL) were added to the upper wells of the chemotaxis chambers together with HFL-1 cells. (*a*) SB203580, (*b*) SB202190; HFn (20 μg/ml) was used as the chemoattractant. Vertical axis: fibroblast migration expressed as percentage of control. Data are presented as the mean + SEM from triplicate cultures each assayed for migration in triplicate. *$P < .05$

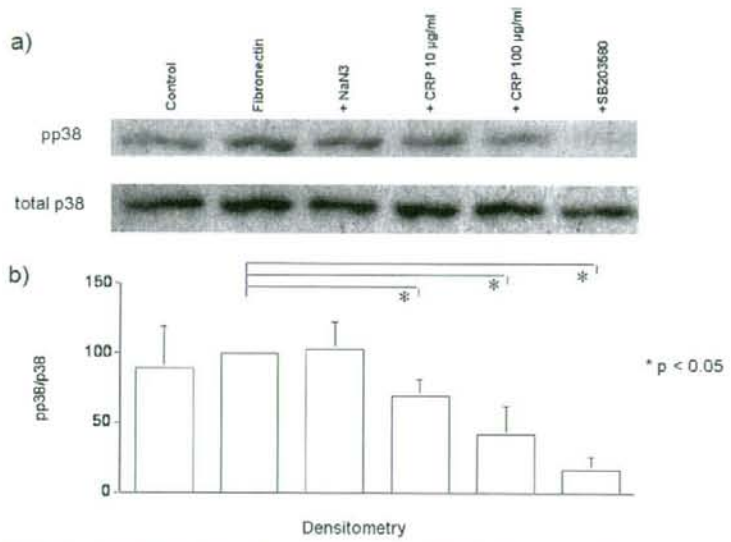

FIGURE 5 Western blot analysis of phosphorylated p38 MAPK. The protein samples were prepared after the 10-minute incubation at described conditions. (*a*) The representative result from 3 separate experiments. (*b*) The densities of phosphorylated p38 were divided by the density of total p38. Data are presented as the mean ± SEM from separate triplicate experiments. $^*P < .05$

(Figure 2). The concentration used in this study was similar to in vivo concentrations, suggesting that this pathway has relevance in the clinical events. The inhibitory effect of the CRP increased with time (Figure 3). Furthermore, our data suggested that this biological effect of CRP was mediated through inhibition of p38 MAPK (Figure 5).

In the process of wound repair, fibroblast migration, proliferation, and contraction are essential events. If these fibroblast functions do not work exactly, inaccurate repair remodeling would be proceeded. Remodeling of the lung structure is a major part of the pathogenesis of several lung diseases, including pulmonary fibrosis [17], chronic obstructive lung disease [18, 19], and bronchial asthma [20, 21]. It is believed that the fibrosis that often characterizes lung remodeling results from excess migration, proliferation and activation of fibroblasts. Thus modulation of fibroblast migration may be an option for controlling the excess development of fibrosis.

C-reactive protein is an acute phase protein and is clinically utilized as a nonspecific marker of inflammation. Over the past few years, several reports have demonstrated that the level of CRP in the serum reflects the severity of several diseases, including atherosclerosis [22] and cardiac vascular disease [23]. Moreover, CRP induces release of a number of mediator proteins from

target cells [24], attenuates nitric oxide (NO) production [7], and inhibits migration of neutrophils [5, 6]. These reports suggest that CRP is not only an inflammatory marker but is potentially also an important mediator of disease. However, it remains largely unknown if CRP modulates any biological processes in the lung.

p38 MAPK activation is involved in HFn-induced migration. Fibronectin is believed to plays an important role in the regulation of fibroblast recruitment and accumulation [25, 26]. However, it remains unclear whether or not p38 MAPK activation is involved in HFn-induced migration. In the present study, we showed that (1) pharmacological inhibition of p38 MAPK significantly blocked cell migration, and that (2) CRP inhibited p38 MAPK activation as well as cell migration. These findings strongly suggest that p38 MAPK plays a pivotal role in HFn-induced fibroblast migration, and a possible role in CRP-reduced cell migration. CRP-modulated fibroblast migration may occur, at least in part, via inhibition of the p38 MAPK pathway. We have no direct evidences to support this hypothesis, because the effects of both CRP and p38 MAPK inhibitors showed an inhibitory effect on cell migration. The report that CRP inhibits chemotactic peptide–induced p38 MAPK activity in neutrophils [6] might support our hypothesis.

p38 MAPK inhibition might be a candidate of novel therapeutic strategy in fibrotic processes of the lung. Rousseau and associates [27] reported that fibroblasts derived from p38 MAPK–lacking mice showed a markedly reduced migratory response to chemoattractants, showing an inevitable role of p38 MAPK in cell migration. Inhibition of p38 MAPK reduces airway inflammation of patient in cystic fibrosis [28]. Therefore, it might be a good treatment for fibrotic lung disease to inhibit p38 MAPK activation.

C-reactive protein effect was not through the protein kinase A pathway. Our previous studies indicate that the mediator that decreases the lung fibroblast migration are related to the protein kinase A pathway [12, 29, 30]. We have also tried to confirm whether CRP effect was by way of the protein kinase A pathway. The protein kinase A inhibitor KT5720 did not block the CRP effect.

It is CRP itself that decreases the movement of lung fibroblast. Several in vitro studies have suggested that CRP induces the inflammatory response directly. However, there is the possibility that the effects are caused by biologically active contaminants of commercially available CRP such as endotoxin and sodium azide [14, 15, 31]. First of all, we examined the effect of LPS, which was known as endotoxin on lung fibroblast migration. LPS had no effects on the HFL-1 migration (Figure 1*a*). Second, we examined the effect of sodium azide. Even at the highest concentration of sodium azide examined, there was no effect on fibroblast migration (Figure 1*b*). Furthermore, we compared the effects of azide- and endotoxin-free CRP and conventional CRP, which is not free from azide and endotoxin. We could demonstrate similar results (Figure 2). These results indicated that the decreased the

fibroblast migration was not due to endotoxin or sodium azide but CRP itself.

In summary, the inhibitory effect of CRP on cell migration and p38 MAPK activation in human lung fibroblasts shown here suggest that CRP might be an endogenous modulator of lung fibrosis. Further studies are necessary for better understanding the role of CRP in lung fibrosis and wound healing.

Declaration of interest: This work was supported in part by grants-in-aid for Scientific Research from the Ministry of Education, Science, Sports, Culture and Technology of Japan, a grant to the Respiratory Failure Research Group from the Ministry of Health, Labour and Welfare, Japan, and grants-in-aid for Comprehensive Research on Aging and Health from the Ministry of Health, Labour and Welfare, Japan. The authors thank Makiko Kase for her excellent technical assistance.

REFERENCES

[1] Gabay C, Kushner I: Acute-phase proteins and other systemic responses to inflammation. N Engl J Med. 1999;340;448–454.

[2] Griselli M, Herbert J, Hutchinson WL, Taylor KM, Sohail M, Krausz T, Pepys MB: C-reactive protein and complement are important mediators of tissue damage in acute myocardial infarction. J Exp Med. 1999;190;1733–1740.

[3] Kew RR, Hyers TM, Webster RO: Human C-reactive protein inhibits neutrophil chemotaxis in vitro: possible implications for the adult respiratory distress syndrome. J Lab Clin Med. 1990;115;339–345.

[4] Heuertz RM, Webster RO: Role of C-reactive protein in acute lung injury. Mol Med Today. 1997;3;539–545.

[5] Zhong W, Zen Q, Tebo J, Schlottmann K, Coggeshall M, and Mortensen RF: Effect of human C-reactive protein on chemokine and chemotactic factor-induced neutrophil chemotaxis and signaling. J Immunol. 1998;161;2533–2540.

[6] Heuertz RM, Tricomi SM, Ezekiel UR, Webster RO: C-reactive protein inhibits chemotactic peptide-induced p38 mitogen-activated protein kinase activity and human neutrophil movement. J Biol Chem. 1999;274;17968–17974.

[7] Verma S, Wang CH, Li SH, Dumont AS, Fedak PW, Badiwala MV, Dhillon B, Weisel RD, Li RK, Mickle DA, Stewart DJ: A self-fulfilling prophecy: C-reactive protein attenuates nitric oxide production and inhibits angiogenesis. Circulation. 2002;106;913–919.

[8] Wang CH, Li SH, Weisel RD, Fedak PW, Dumont AS, Szmitko P, Li RK, Mickle DA, Verma S: C-reactive protein upregulates angiotensin type 1 receptors in vascular smooth muscle. Circulation 2003;107;1783–1790.

[9] Gould JM, Weiser JN: Expression of C-reactive protein in the human respiratory tract. Infect Immun. 2001;69;1747–1754.

[10] Arase Y, Ikeda K, Tsubota A, Saitoh S, Suzuki Y, Kobayashi M, Suzuki F, Someya T, Akuta N, Hosaka T, Kobayashi M, Kumada H: Usefulness of serum KL-6 for early diagnosis of idiopathic pulmonary fibrosis in patients with hepatitis C virus. Hepatol Res. 2003;27;89–94.

[11] Boyden S: The chemotactic effect of mixtures of antibody and antigen on polymorphonuclear leukocytes. J Exp Med. 1962;115;453–466.

[12] Kohyama T, Liu XD, Wen FQ, Kim HJ, Takizawa H, Rennard SI: Prostaglandin D2 inhibits fibroblast migration. Eur Respir J. 2002;19;684–689.

[13] Yamauchi Y, Okazaki H, Desaki M, Kohyama T, Kawasaki S, Yamamoto K, Takizawa H: Methotrexate induces interleukin-8 production by human bronchial and alveolar epithelial cells. Clin Sci (Lond). 2004;106;619–625.

[14] Liu C, Wang S, Deb A, Nath KA, Katusic ZS, McConnell JP, Caplice NM: Proapoptotic, antimigratory, antiproliferative, and antiangiogenic effects of commercial C-reactive protein on various human endothelial cell types in vitro: implications of contaminating presence of sodium azide in commercial preparation. Circ Res. 2005;97;135–143.
[15] VanUffelen BE, Van der Zee J, de Koster BM, VanSteveninck J, and Elferink JG: Sodium azide enhances neutrophil migration and exocytosis: involvement of nitric oxide, cyclic GMP and calcium. Life Sci. 1998;63;645–657.
[16] Kohyama T, Liu X, Wen FQ, Kim HJ, Takizawa H, Rennard SI: Potentiation of human lung fibroblast chemotaxis by the thromboxane A(2) analog U-46619. J Lab Clin Med. 2002;139;43–49.
[17] Parra ER, David YR, da Costa LR, Ab'Saber A, Sousa R, Kairalla RA, de Carvalho CR, Filho MT, Capelozzi VL: Heterogeneous remodeling of lung vessels in idiopathic pulmonary fibrosis. Lung 2005;183;291–300.
[18] Chung KF: The role of airway smooth muscle in the pathogenesis of airway wall remodeling in chronic obstructive pulmonary disease. Proc Am Thorac Soc. 2005;2;347–354.
[19] Hogg JC, Chu F, Utokaparch S, Woods R, Elliott WM, Buzatu L, Cherniack RM, Rogers RM, Sciurba FC, Coxson HO, Pare PD: The nature of small-airway obstruction in chronic obstructive pulmonary disease. N Engl J Med. 2004;350;2645–2653.
[20] Lavigne MC, Thakker P, Gunn J, Wong A, Miyashiro JS, Wasserman AM, Wei SQ, Pelker JW, Kobayashi M, Eppihimer MJ: Human bronchial epithelial cells express and secrete MMP-12. Biochem Biophys Res Commun. 2004;324;534–546.
[21] Karagiannidis C, Hense G, Martin C, Epstein M, Ruckert B, Mantel PY, Menz G, Uhlig S, Blaser K, Schmidt-Weber CB: Activin A is an acute allergen-responsive cytokine and provides a link to TGF-beta-mediated airway remodeling in asthma. J Allergy Clin Immunol. 2006;117;111–118.
[22] Sun H, Koike T, Ichikawa T, Hatakeyama K, Shiomi M, Zhang B, Kitajima S, Morimoto M, Watanabe T, Asada Y, Chen YE, Fan J: C-reactive protein in atherosclerotic lesions: its origin and pathophysiological significance. Am J Pathol. 2005;167;1139–1148.
[23] Danesh J, Wheeler JG, Hirschfield GM, Eda S, Eiriksdottir G, Rumley A, Lowe GD, Pepys MB, Gudnason V: C-reactive protein and other circulating markers of inflammation in the prediction of coronary heart disease. N Engl J Med. 2004;350;1387–1397.
[24] Cermak J, Key NS, Bach RR, Balla J, Jacob HS, Vercellotti GM: C-reactive protein induces human peripheral blood monocytes to synthesize tissue factor. Blood 1993;82;513–520.
[25] Kawamoto M, Matsunami T, Ertl RF, Fukuda Y, Ogawa M, Spurzem JR, Yamanaka N, Rennard SI: Selective migration of α-smooth muscle actin-positive myofibroblasts toward fibronectin in the Boyden's blindwell chamber. Clin Sci. 1997;93;355–362.
[26] Mattoli S, Colotta F, Fincato G, Mezzetti M, Mantovani A, Patalano F, Fasoli A: Time course of IL1 and IL6 synthesis and release in human bronchial epithelial cell cultures exposed to toluene diisocyanate. J Cell Physiol. 1991;149;260–268.
[27] Rousseau S, Dolado I, Beardmore V, Shpiro N, Marquez R, Nebreda AR, Arthur JS, Case LM, Tessier-Lavigne M, Gaestel M, Cuenda A, Cohen P: CXCL12 and C5a trigger cell migration via a PAK1/2-p38alpha MAPK-MAPKAP-K2-HSP27 pathway. Cell Signal. 2006;18:1897–1905.
[28] Raia V, Maiuri L, Ciacci C, Ricciardelli I, Vacca L, Auricchio S, Cimmino M, Cavaliere M, Nardone M, Cesaro A, Malcolm J, Quaratino S, Londei M: Inhibition of p38 mitogen activated protein kinase controls airway inflammation in cystic fibrosis. Thorax. 2005;60;773–780.
[29] Kohyama T, Ertl RF, Valenti V, Spurzem J, Kawamoto M, Nakamura Y, Veys T, Allegra L, Romberger D, Rennard SI: Prostaglandin E(2) inhibits fibroblast chemotaxis. Am J Physiol Lung Cell Mol Physiol. 2001;281;L1257–L1263.
[30] Kohyama T, Liu X, Kim HJ, Kobayashi T, Ertl RF, Wen FQ, Takizawa H, Rennard SI: Prostacyclin analogs inhibit fibroblast migration. Am J Physiol Lung Cell Mol Physiol. 2002;283;L428–L432.
[31] Taylor KE, Giddings JC, van den Berg CW: C-reactive protein-induced in vitro endothelial cell activation is an artefact caused by azide and lipopolysaccharide. Arterioscler Thromb Vasc Biol. 2005;25;1225–1230.

British Journal of Pharmacology (2009), **, **–**

0007-1188/09
www.brjpharmacol.org

RESEARCH PAPER

Eicosapentaenoic acid inhibits voltage-gated sodium channels and invasiveness in prostate cancer cells

T Nakajima[1], N Kubota[1,2], T Tsutsumi[2], A Oguri[3], H Imuta[1], T Jo[4], H Oonuma[4], M Soma[5], K Meguro[3], H Takano[1], T Nagase[4] and T Nagata[4]

[1]*Department of Ischemic Circulatory Physiology, The University of Tokyo, Tokyo, Japan,* [2]*Division of Cardiology, Showa University Fujigaoka Hospital, Yokohama, Japan,* [3]*Department of Cardiovascular Medicine, The University of Tokyo, Tokyo, Japan,* [4]*Department of Respiratory Medicine, The University of Tokyo, Tokyo, Japan, and* [5]*Pharmacovigilance, Mochida Pharmaceutical, Tokyo, Japan*

Background and purpose: The voltage-gated Na^+ channels (Na_v) and their corresponding current (I_{Na}) are involved in several cellular processes, crucial to metastasis of cancer cells. We investigated the effects of eicosapentaenoic (EPA), an omega-3 polyunsaturated fatty acid, on I_{Na} and metastatic functions (cell proliferation, endocytosis and invasion) in human and rat prostate cancer cell lines (PC-3 and Mat-LyLu cells).
Experimental approach: The whole-cell voltage clamp technique and conventional/quantitative real-time reverse transcriptase polymerase chain reaction analysis were used. The presence of Na_v proteins was shown by immunohistochemical methods. Alterations in the fatty acid composition of phospholipids after treatment with EPA and metastatic functions were also examined.
Key results: A transient inward Na^+ current (I_{Na}), highly sensitive to tetrodotoxin, and Na_v proteins were found in these cells. Expression of $Na_v1.6$ and $Na_v1.7$ transcripts (SCN8A and SCN9A) was predominant in PC-3 cells, while $Na_v1.7$ transcript (SCN9A) was the major component in Mat-LyLu cells. Tetrodotoxin or synthetic small interfering RNA targeted for SCN8A and SCN9A inhibited metastatic functions (endocytosis and invasion), but failed to inhibit proliferation in PC-3 cells. Exposure to EPA produced a rapid and concentration-dependent suppression of I_{Na}. In cells chronically treated (up to 72h) with EPA, the EPA content of cell lipids increased time-dependently, while arachidonic acid content decreased. Treatment of PC-3 cells with EPA decreased levels of mRNA for SCN9A and SCN8A, cell proliferation, invasion and endocytosis.
Conclusion and implications: Treatment with EPA inhibited I_{Na} directly and also indirectly, by down-regulation of Na_v mRNA expression in prostate cancer cells, thus inhibiting their metastatic potential.
British Journal of Pharmacology (2009) doi:10.1111/j.1476-5381.2008.00059.x

Keywords: voltage-gated sodium channels; prostate carcinoma cell; eicosapentaenoic acid; SCN9A; SCN8A; RT-PCR; invasion; endocytosis; proliferation

Abbreviations: EPA, eicosapentaenoic acid; FBS, fetal bovine serum; I_{Na}, Na^+ current; Na_v, voltage-gated Na^+ channel; NMDG, N-methyl-D-glucamine; PUFA, polyunsaturated fatty acid; RT-PCR, reverse transcriptase polymerase chain reaction; siRNA, synthetic small interfering RNA; TTX, tetrodotoxin

Introduction

The therapy of prostate cancer including the use of hormone-based drugs has progressed over recent years, but prostate cancer is still one of the leading causes of cancer deaths in the world. Therefore, new therapeutic strategies to prevent prostate cancer, to inhibit its progression and metastasis are needed. Epidemiological studies show clear geographical variations in the incidence of this disease (Parkin *et al.*, 2005), with it being more common in the developed countries such as North America and Europe, compared with developing countries. And, within the developed countries, considerable differences of the mortality rates exist; North America and Europe have high mortality rates as compared with Japan and other Asian countries (Breslow *et al.*, 1977). However, the frequency of latent prostate carcinoma diagnosed at autopsy is as common in Asian countries as in Western countries (Dunn, 1975). In addition, the consumption of a diet rich in fat tends to increase the risk of developing prostate carcinoma (Shennan and Bishop, 1974) and immigrants from Poland and Japan to the Western countries show a significant increase in the risk of developing prostate cancer (Haenszel and Kurihara, 1968; Armstrong and Doll, 1975). These findings implicate environmental factors, probably diet, as significant

Correspondence: T Nakajima, Department of Ischemic Circulatory Physiology, University of Tokyo, 7-3-1 Hongo, Bunkyo-ku, Tokyo 113-8655, Japan. E-mail: masamasa@pb4.so-net.ne.jp
Received 21 July 2008; revised 22 September 2008; accepted 30 September 2008

contributing factors enhancing oncogenesis and the growth and metastasis of prostate cancer. There is also growing evidence that omega-6 (ω-6) polyunsaturated fatty acids (PUFAs) promote prostate cancer growth, whereas ω-3 PUFA, from marine foods, are inhibitory (Rose, 1997; Larsson *et al.*, 2004; Leitzmann *et al.*, 2004), and high blood levels of ω-3 PUFA are associated with a reduced risk of prostate cancer (Chavarro *et al.*, 2007). Thus, excessive amounts of ω-6 PUFAs and a higher ratio of ω-6/ω-3 PUFAs in prostate cells may contribute to an increased incidence of prostate cancer. Consequently, increasing dietary ω-3 PUFAs, such as eicosapentaenoic acid (EPA), and decreasing the ω-6/ω-3 ratios of prostate cells appears to be a feasible approach to reduce the risk and control growth of prostate cancer an of its metastasis, resulting in increased survival (Larsson *et al.*, 2004; Kelavkar *et al.*, 2006; Chavarro *et al.*, 2007). However, the basic mechanisms underlying these protective effects of EPA remain undefined.

Ion channels play essential roles in cell function, that is, cell growth, metastasis and secretion in many types of cells, including cancer cells. EPA has been reported to modulate membrane-bound proteins such as ion channels, that is, voltage-gated Ca^{2+} channels (Xiao *et al.*, 1997) and voltage-gated Na^+ channels (Na_v) (Xiao *et al.*, 1995; 1998; Kang and Leaf, 1996; Jo *et al.*, 2005). The binding sites of EPA on Na_v have been proposed to be located on the cytoplasmic segment of the Na^+ channel, in the α-subunit linking transmembrane repeats III and IV (Xiao *et al.*, 2001). Thus, Na_v appears to be an important target protein for EPA. A number of papers have reported that the up-regulation of the current (I_{Na}) carried by Na_v channels is observed in malignant tumours of prostate, as compared with non-malignant tumours, and contributes to the progression and metastasis by enhancing a number of metastatic cell functions such as invasion, secretion and endocytosis (Grimes *et al.*, 1995; Fraser *et al.*, 2000; 2003; Anderson *et al.*, 2003; Bennett *et al.*, 2004; Krasowska *et al.*, 2004; Brackenbury and Djamgoz, 2006). So far, 10 types of α-subunit in Na channels, referred to as SCN1A to SCN11A, have been identified (Goldin, 1999; 2002; nomenclature follows Alexander *et al.*, 2008). The protein $Na_v1.7$ encoded by the SCN9A gene has been reported to a major carrier of the functional I_{Na} expressed in prostate cancer cells (Diss *et al.*, 2001; 2005). However, the effects of EPA on I_{Na} in prostate cancer cells have not been investigated.

To elucidate the protective effects of EPA on prostate cancer, the effects of EPA on I_{Na} were examined by the whole-cell patch-clamp technique and effects on the Na_v transcripts by real-time reverse transcriptase polymerase chain reaction (RT-PCR) analysis, in human and rat prostate cancer cells (PC-3 and Mat-LyLu cell lines). The alterations in fatty acid composition of cellular phospholipids after treatment with EPA and functions of prostate cancer cells contributing to metastasis (proliferation, invasion and endocytosis) were also investigated.

Methods

Cell preparation

PC-3 human prostate epithelial tumour cell lines and Mat-LyLu rat epithelial tumour cell lines were obtained from JCRB cell bank (Osaka, Japan) and European Collection of Cell Cultures (ECACC, Wiltshire, UK) respectively. PC-3 cells were grown in Kaighn's modification of Ham's F12 medium (F12K) with 7% fetal bovine serum (FBS) in an atmosphere of 5% CO_2 and 95% air at 37°C. Mat-LyLu cancer cells were cultured in RPMI 1640 medium containing 2 mmol·L^{-1} glutamine and 10% FBS. When cells became confluent, they were subcultured in the same medium. At confluence, the cells were passaged by using 0.05% trypsin in 0.02% EDTA. Medium was replaced twice weekly.

Solutions and drugs

The composition of the control extracellular Tyrode solution was as follows (in mmol·L^{-1}): NaCl 136.5, KCl 5.4, $CaCl_2$ 1.8, $MgCl_2$ 0.53, glucose 5.5 and HEPES-NaOH buffer 5.5 (pH 7.4). To block K^+ currents, the patch pipette contained (in mmol·L^{-1}): CsCl 140, EGTA 10, $MgCl_2$ 2, Na_2ATP 3, guanosine-5'-triphosphate (GTP, sodium salt, Sigma) 0.1 and HEPES-CsOH buffer 5 (pH 7.2). In addition, 4-aminopyridine (4-AP, 4 mmol·L^{-1}), tetraethylammonium (2 mmol·L^{-1}) and Ba^{2+} (1 mmol·L^{-1}) were added to the control solution to block K^+ current and record I_{Na}. Nifedipine, 4-AP, TEA, tetrodotoxin (TTX) and cis-5,8,11,14,17-eicosapentaenoic acid (EPA, Na salt) were obtained from Sigma Chemicals Co. EPA was dissolved in water just before use.

Recording technique and data analysis

Membrane currents were recorded with tight-seal whole-cell clamp techniques by using a patch-clamp amplifier (EPC-7, List Electronics, Darmstadt, Germany) (Hamill *et al.*, 1981; Nakajima *et al.*, 1999). The heat-polished patch electrode had tip resistance of 3–5 MΩ. All data were acquired, stored and analysed on Power Macintosh 7100/80 by using the PULSE + PULSEFIT software (HEKA Electronic) and Igor PRO (Wave Metrics, Lake Oswego, OR) as previously described (Terasawa *et al.*, 2002). All experiments were performed at room temperature (20–25°C). The steady-state inactivation of I_{Na} was estimated by using double-pulse protocols. Conditioning voltage pulses (500 ms in duration) of various membrane potentials between –80 and +20 mV were applied from a holding potential of –80 mV. At 2 ms after the end of each conditioning pulse, a test pulse of +0 mV (300 ms in duration) was applied to elicit I_{Na}. The ratio of I_{Na} amplitudes, with and without conditioning pulses, was plotted against each conditioning voltage.

Analysis of fatty acid composition

PC-3 cells were incubated for 2.7–72 h in medium containing 30 μmol·L^{-1} EPA, and the medium was changed every other day. The cells were harvested by trypsinization, centrifuged at 2000× *g* for 15 min at 4°C, and then washed twice and resuspended at a cell density of 2×10^7 cells·mL^{-1} in 20 mmol·L^{-1} phosphate buffer (pH 7.4) and then sonicated (10 watt for 2 min and then 40 watt for 30 s on ice). The lipids in the cell sonicate were analysed as described earlier (Asano *et al.*, 1998). Briefly, lipids were extracted with chloroform–methanol solution (2:1, v·v^{-1}) in the presence of butylated hydroxytoluene. Fatty acid composition of cell phospholipids was determined by gas chromatography after separation of

phospholipid fraction by using aminopropyl-bonded phase columns.

RNA extraction, RT-PCR and real-time quantitative RT-PCR

Total cellular RNA was extracted by using ISOGEN (Nippon Gene, Tokyo, Japan). For RT-PCR, complementary DNA (cDNA) was synthesized from 1 μg of total RNA with reverse transcriptase with random primers (Toyobo, Osaka, Japan) as previously described (Jo *et al.*, 2004). The reaction mixture was then subjected to PCR amplification with specific forward and reverse oligonucleotide primers for 35 cycles consisting of heat denaturation, annealing and extension. PCR products were size-fractionated on 2% agarose gels and visualized under UV light. Primers were chosen based on the sequence of human SCN1–6A and 8–9A and rat SCN1A–6A and 8–9A as shown in Table 1. Real-time quantitative RT-PCR was performed with the use of real-time Taq-Man technology and a sequence detector (ABI PRISM® 7000, Applied Biosystems, Foster City, CA, USA) (Jo *et al.*, 2004). Gene-specific primers and Taq-Man probes were used to analyse transcript abundance. The 18S ribosomal RNA level was analysed as an internal control and used to normalize the values for transcript abundance of SCN family genes (SCN1–6A, 8A, 9A).

Immunocytochemistry

Immunocytochemical analyses were performed on the cells by using anti-PanNa$_v$ (Alomone Labs, Jerusalem, Israel), a rabbit polyclonal antibody against a peptide conserved in all Na$_v$ isoforms, anti-Na$_v$1.6 and anti-Na$_v$1.7 (Alomone Labs, Jerusalem, Israel). The cells were cultured on Lab-Tek Chamber Slide Glass (Nalge Nunc International, Naperville, IL, USA), fixed with 2% paraformaldehyde in PBS for 30 min and then blocked for 10 min with 2% horse serum in PBS. The cells were incubated for 60 min with the primary antibodies diluted with 0.01% Triton X and 0.01% NaN_3 in PBS. For negative controls, cells were treated without antibody. Alexa-Fluor-488-conjugated labelled donkey anti-rabbit IgG antibody (Molecular Probes, A21206) was used to visualize the channel expression. The cells were also stained with Hoechst 33 258 (Sigma Aldrich) to visualize nuclei. A confocal laser scanning microscope (Olympus FluoView FV300, Olympus Co., Tokyo, Japan) was used for observations.

Transfection of synthetic small interfering RNA (siRNA)

SCN8A and SCN9A siRNA and non-silencing (negative control) siRNAs, as described in Table 1, were purchased from Qiagen (Cambridge, MA, USA). They were transfected into PC-3 cells to a final concentration of 5 nmol·L^{-1}, by using the HiPerFect Transfection Reagent (5 μL·mL^{-1} culture; Qiagen) according to the instructions of the manufacturer. Transfected cells were incubated for 48 h in an atmosphere of 5% CO_2 and 95% air at 37°C before each experiment. Then, analysis of mRNA by using real-time RT-PCR and the functions of the cells were performed. Rhodamine-conjugated siRNA was used to confirm the transfection of siRNA by using Nikon ECLISE TE200-u.

Proliferation assay

Cell proliferation was assessed by the Cell Titer 96 Aqueous kit (Promega, Madison, WI, USA). The prostate cancer cells were plated in 96-well plates (Becton Dickinson Labware, Franklin Lakes, NJ, USA) at a density of 1×10^4 cells per well. On the next day, experimental media with TTX, EPA or siRNA were added. The plates were then incubated for 24 or 48 h, after which the

Table 1 PCR primers used for amplification of voltage-gated Na$^+$ channel genes and synthetic small interfering RNA (siRNA) for SCN8A and 9A

Gene symbol (human/rat)	*Channel*	*Size (bp)*		*Sequence ('5-'3)*	
hSCN1A (rSCN1A)	Na$_v$1.1	298 (436)	sense	GAC AGC ATC AGG AGG AAA GG	(GCAAGCTGTCCGCTGGTAATATA)
			antisense	TGG TCT GAC TCA GGT TGC TG	(AGTGATCGTGATATCAACCTGAAG)
hSCN2A (rSCN2A)	Na$_v$1.2	194 (494)	sense	ATC CAG AGG GCT TAC AGA CG	(GCTGCAGCTCTCCATTCACACAC)
			antisense	ATC ATA CGA GGG TGG AGA CG	(GGCTAAACAATACTGCAGGGAAAA)
hSCN3A (rSCN3A)	Na$_v$1.3	354 (422)	sense	AAT TCT GTG GGG GCT CTA GG	(TATCCGTGTCAACTGGACTCTAAG)
			antisense	AGC AGC AAG GTT GTC TGA GC	(GATTACTGGAGAAACTTGTGGACT)
hSCN4A (rSCN4A)	Na$_v$1.4	502 (407)	sense	CAG GCA TCT TCA CAG CAG AG	(GCCTGCGCTCTCTGACTTG)
			antisense	ACC ATG AGG AAG ACG GTG AG	(CCTGACATTGGTACCCGG)
hSCN5A (rSCN5A)	Na$_v$1.5	618 (501)	sense	ACC ATC GTG AAC AAC AAG AGC C	(GCCTAGTCTGGAACTCCCTGGAC)
			antisense	GGC AGC CAG CTT GAC AAT ACA C	(ACATCTCCAGAGAGCTACGGGACAC)
hSCN6A (rSCN6A)	Na$_x$	449 (692)	sense	AAG AGG TGT CTG GGC AGG AT	(AAAGGACCAAAGGTGTTCCATGATCTGATG)
			antisense	GAC CAG CAT CTG TCC TGT TG	(CCGCTCATCCTTTCCCATCACTCTTTTCGT)
hSCN8A (rSCN8A)	Na$_v$1.6	599 (401)	sense	GAG GTG AAG CCT CTG GAT GA	(TTCAATGCGGTTTCCATCCT)
			antisense	CGG ATG GTC TTT CTC TGC TC	(GACTGCAGGCCATGGTTCA)
hSCN9A (rSCN9A)	Na$_v$1.7	403 (402)	sense	GAG GCC TGT TTC ACA GAT GG	(TCAGCGTGCTTACAGACGGTA)
			antisense	TGG GGC CAA GAT CTG AGT AG	(CTAATGGCTGTGCTGCCTTTG)

siRNA (human)	Sequence
SCN8A_2 (82)	AACAACCAACTAATTGACTAA
SCN8A_4 (84)	CCCAGTTCATTGAGTACTGTA
SCN8A_6 (86)	CAGAGGGATACCAGTGTATGA
SCN9A_1 (91)	TAGGCTAATGACCCAAGATTA
SCN9A_4 (94)	CGGCAGCGGCTGAATATACAA
control(non-silence)	AATTCTCCGAACGTGTCACGT

tetrazolium salt and dye solution was added and colour development was allowed to proceed for 1 h at 37°C, 5% CO_2. Each plate was then read at an absorbance of 490 nm.

Invasion assay

Matrigel invasion chambers were prepared according to the manufacturer's instructions (Becton Dickinson Labware, MA) by coating Matrigel on the 8 μm pore membrane of the culture inserts for 24-well plates (Falcon). A 0.5 mL aliquot of PC-3 cell suspension at 1×10^5 cells·mL^{-1} treated with or without siRNA for 48 h was seeded on the upper chamber and incubated at 37°C in a humidified chamber. Seven per cent FBS with or without TTX and EPA was added to the upper compartment. After migration for 24 h at 37°C, cells were removed from the upper compartment. The number of invasive PC-3 cells on the lower surface of the filter membrane was determined by Diff Quik staining (Siemens, IL) and counted at a magnification of ×100. The percentage invasion was calculated as the ratio of the number of invasive cells in the presence of TTX, EPA or siRNA, relative to that in the absence of the drug.

Endocytosis assay

PC-3 cells were placed in Eppendorf tubes at a density of 1×10^5 cells per tube in Tyrode solution and left to equilibrate for 10–15 min. The solution was then replaced by 100 μL of Tyrode solution containing 0.5 mg·mL^{-1} horseradish peroxidase (HRP) type IV (Sigma-Aldrich). The cells were incubated in an atmosphere of 5% CO_2 and 95% air at 37°C for 60 min with and without TTX, EPA or siRNA as previously described (Onganer and Djamgoz, 2005). A background, which indicates endogenous peroxidase activity, was measured with normal Tyrode solution. After the incubation, the cells were rinsed three times to remove all extracellular HRP. In order to release the HRP contents of the cells, 120 μL of lysis buffer (made by serially adding 0.9 g NaCl, 10 mL 10% NP-40 and 2.5 mL 10% Na-deoxycholate to a solution of 0.79 g Tris base in 75 mL distilled water and adding 1 mL of 100 mmol·L^{-1} EDTA and completing the volume to 100 mL with distilled water) was added to the cell pellet. Immediately afterwards, diaminobenzidine (0.5 mg·mL^{-1}) and hydrogen peroxide (0.01%) in 120 μL of 1 mol·L^{-1} Tris buffer (pH 7.4) were added, and the reaction solutions were transferred to a 96-well plate. The density of the colour reaction was measured at 570 nm on a plate reader (Bio-Rad Laboratories Inc, Helcules, CA, USA), and the absorbance was taken to represent the endocytotic activity.

Data analysis

All values are expressed as means ± SEM. Student's paired *t*-test was used to compare two sets of data from the same subjects. Comparison of time courses of parameters was analysed by one-way ANOVA for repeated measures. When differences were indicated, a Bonferroni's comparison was used to determine significance. Differences were considered significant if $P < 0.05$.

Results

EPA inhibits Na^+ current in prostate cancer cells

Figure 1A,B show I_{Na} in prostate cancer cells. The cells were held at –80mV, and the command voltage pulses (50 ms in duration) were applied to +0 mV. A fast transient inward current could be elicited in both human PC-3 cancer cells (Figure 1A) and Mat-LyLu rat cancer cells (Figure 1B). TTX (1 μmol·L^{-1}, Figure 1A,B) or replacement of extracellular Na^+ with N-methyl-D-glucamine (NMDG; Figure 1C), an impermeable cation, completely abolished I_{Na}, indicating that the transient inward current was carried by TTX-sensitive Na^+ channels (Na_v), as previously reported for these prostate cancer cell lines (Grimes *et al.*, 1995; Laniado *et al.*, 1997; Fraser *et al.*, 2003; Brackenbury and Djamgoz, 2006).

The typical current data recorded at each membrane potential and current–voltage (I–V) relations measured at the peak of the inward current are shown for Mat-LyLu cells (Figure 1D,E). At potentials more positive than –40 mV, I_{Na} was elicited (Figure 1A). The peak amplitude of the inward current was observed at approximately –10 mV. Figure 1F shows the steady-state inactivation curve for I_{Na}. The relation between membrane potentials and the h_∞ value (Figure 1F) was fitted to the following equation (Boltzmann equation) by using the least-squares methods: $I(V)/I_{max} = 1/\{1 + \exp[(V - V_h)k^{-1}]\}$, where V is the membrane potential in mV, V_h is the membrane potential at half maximum, and k is the slope factor. The value of V_h and k was –61 ± 6 mV and 7.9 ± 4 mV ($n = 4$) respectively.

The effects of TTX on I_{Na} in Mat-LyLu cells are shown in Figure 2A,B. The cells were held at –80 mV, and the command pulses to +0 mV (50 ms in duration) were applied at 0.1 Hz. Inhibition by TTX was concentration-dependent with an IC_{50} value of 7.0 nmol·L^{-1} ($n = 5$). Extracellular application of EPA (30 μmol·L^{-1}) also rapidly inhibited I_{Na}, and this inhibition attained a steady-state level within 2–3 min (Figure 2C). After washing with albumin (0.1%), I_{Na} gradually returned to the control level (Figure 2C). These effects of EPA were concentration-dependent (3–30 μmol·L^{-1}; Figure 2D) and yielded an IC_{50} of approximately 6 μmol·L^{-1} ($n = 5$, Figure 2E).

Expression of mRNA for voltage-gated Na channels in PC-3 cells

The results described above show that a TTX-sensitive Na_v is functional in prostate cancer cells. Therefore, we investigated the expression of mRNA for members of the SCN channel family (SCN1A–9A) in Mat-LyLu cells (Figure 3A) and PC-3 cells (Figure 4A). We did not assay for SCN7A, because SCN6A and 7A are probably encoded by the same gene or for SCN10A or 11A, as I_{Na} carried by these channels is TTX-insensitive (Catterall, 1992). The transcripts of SCN1A, 2A, 6A, 8A and 9A were detected in Mat-LyLu cells (Figure 3A). In PC-3 cells, transcripts of SCN8A and 9A were clearly detected (Figure 4A), and transcripts of SCN2A and 5A were only weakly expressed. The transcripts of SCN1A, 4A and 6A were not detected. The size of SCN cDNA fragments were as predicted, identical to cDNA fragments amplified from reversely transcribed mRNA.

Expression of SCN channel family members (SCN1A–9A) was also investigated by real-time quantitative RT-PCR in

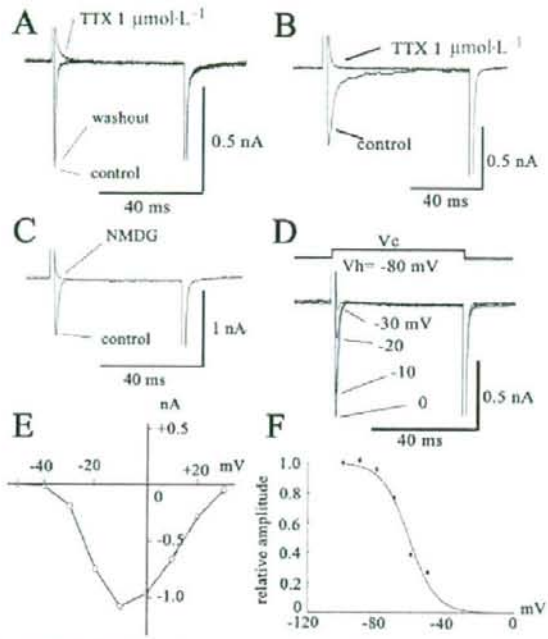

Figure 1 Characteristics of the Na current (I_{Na}) expressed in prostate cancer cells [human prostate cancer cell line (PC-3) and Mat-LyLu rat prostate cancer cell lines]. The cells were held at −80 mV, and command voltage pulses to +0 mV were applied in PC-3 (A) and Mat-LyLu cells (B and C). (C) Effects of replacement of extracellular Na^+ with $NMDG^+$. The current traces in B and C were elicited from a holding potential of −80 mV to +0 mV. In Mat-LyLu cells, the original current traces elicited by depolarizing pulses are indicated in D. The current–voltage (I–V) relations measured at the peak are illustrated in E. The I–V relations are shown after the leakage currents were subtracted. (F) Steady-state inactivation curves for I_{Na} expressed in Mat-LyLu cells. The data obtained from four cells were fitted by a Bolzmann equation. NMDG, N-methyl-D-glucamine; TTX, tetrodotoxin.

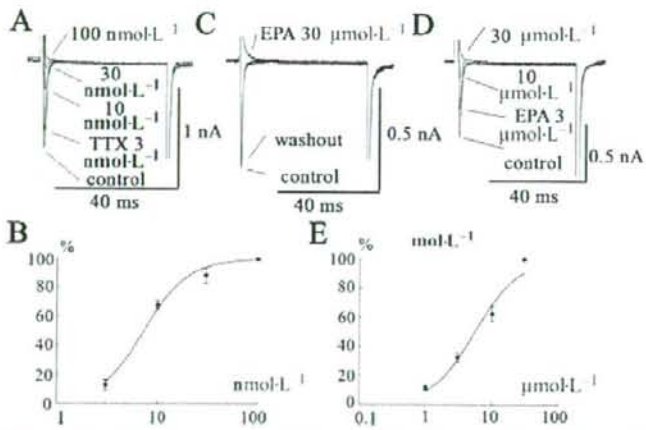

Figure 2 Effects of TTX and EPA on I_{Na} expressed in Mat-LyLu cells. (A) Concentration-dependent inhibition of I_{Na} by TTX. The cells were held at −80 mV, and command voltage-pulses to +0 mV (50 ms in duration) were applied at 0.2 Hz. (B) The inhibitory effect of TTX on the current amplitude measured at the peak is plotted against various concentrations of TTX. Data are shown as means ± SEM ($n = 5$) and fitted to a Michaelis-Menten simple bimolecular model: %inhibition = $100/\{1 + (IC_{50}\ [TTX]^{-1})\}$, where IC_{50} is 50% inhibitory concentration for TTX. The data yielded an IC_{50} value of 7.0 nmol·L^{-1}. (C) Effects of EPA on I_{Na}. The cell was held at −80 mV, and a depolarizing pulse to +0 mV was applied. After washing out with 0.1% albumin, the depressed I_{Na} returned to a control level. (D & E) Concentration-dependent inhibition of I_{Na} by EPA. The data represent a typical recording obtained from five different cells. The inhibitory effect of EPA on the current amplitude measured at the peak is plotted against various concentrations of EPA. Data are shown as means ± SEM ($n = 5$) and fitted using a Hill equation: % inhibition = $100/\{1 + (IC_{50}\ [EPA]^{-1})^n\}$, where n represents Hill coefficient, and IC_{50} is 50% inhibitory concentration for EPA. The data yielded an IC_{50} value of 6 μmol·L^{-1} and n of 1.1. EPA, eicosapentaenoic acid; I_{Na}, Na^+ current; TTX, tetrodotoxin.

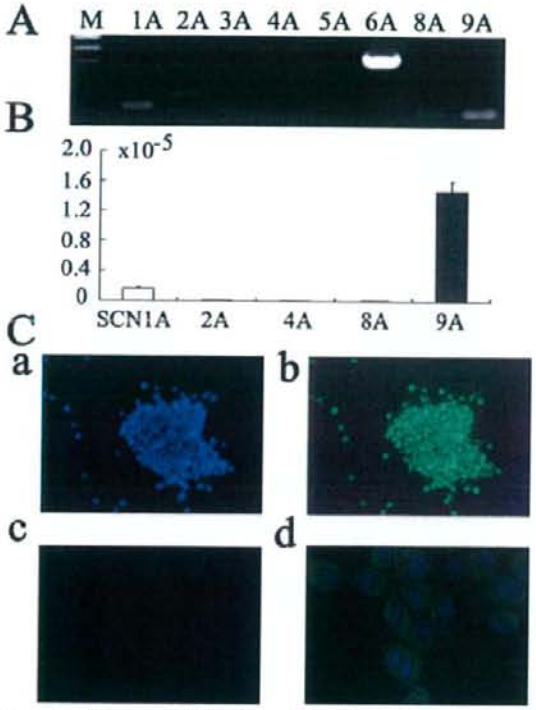

Figure 3 Voltage-gated Na^+ channel proteins in Mat-LyLu rat prostate cancer cell lines. (A) Expression of genes for voltage-gated Na^+ channels, detected by reverse transcriptase polymerase chain reaction (RT-PCR) in Mat-LyLu cells. M, Marker. (B) Summary results of real-time quantitative RT-PCR. The expression levels of SCN channel genes were normalized to those of the 18S ribosomal RNA levels. Data are means ± SEM from six independent samples. (C) Immunocytochemical detection with $PanNa_V$ in Mat-LyLu cells. Staining with Hoechst 33258 to visualize nuclei (Ca), $PanNa_V$ (Cb), negative control (without antibody, Cc), double staining with Hoechst 33258 and $PanNa_V$ (Cd).

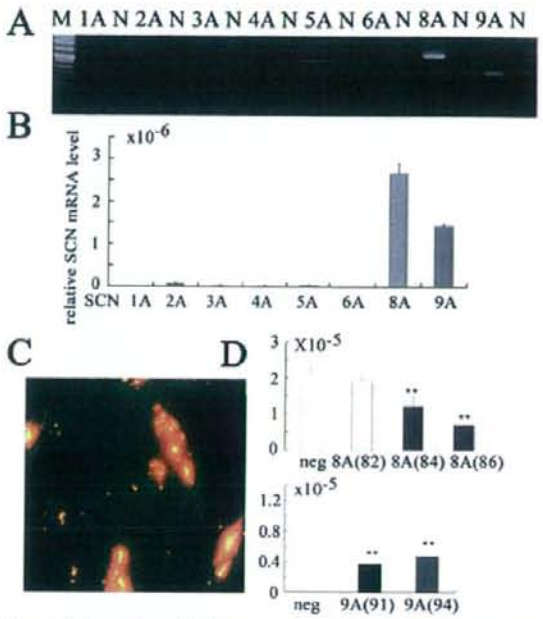

Figure 4 Expression of voltage-gated Na^+ channel genes detected by reverse transcriptase polymerase chain reaction (RT-PCR) in human prostate cancer cell line (PC-3). (A) Results of RT-PCR. M, Marker; N, negative control. (B) Real-time quantitative RT-PCR. The expression levels of SCN channel genes were normalized to those of the 18S ribosomal RNA levels. Summary data are means ± SEM from six independent samples. (C) Transfection of synthetic small interfering RNA (siRNA) for SCN8A mRNA. The transfected siRNA conjugated with rhodamine was visualized under fluorescent microscopy. (D) Expression level of SCN8A and SCN9A mRNA in PC-3 cells transfected with various kinds of siRNA by using real-time quantitative RT-PCR. The numbers in parentheses refer to the different sequences as shown in Table 1 (lower half). $^{**}P < 0.01$ vs. negative control.

Mat-LyLu cells (Figure 3B) and PC-3 cells (Figure 4B). Transcript levels were normalized to 18S ribosomal housekeeping gene. As SCN6A has not been shown to form a functional Na^+ channel (Ogata and Ohishi, 2002), SCN9A appeared to encode for the TTX-sensitive, Na_V in Mat-LyLu cells. On the other hand, in PC-3 cells, expression levels of SCN8A and SCN9A mRNA were much higher than those of SCN2A and 5A, suggesting that SCN8A and SCN9A encode for TTX-sensitive Na_V in PC-3 cells.

Immunocytochemical detection of $PanNa_V$

Expression of Na_V protein was confirmed by immunostaining cultured cells, by using anti-$PanNa_V$ in Mat-LyLu cells (Figure 3Cb), which was consistent with the patch-clamp experiments. No expression of $PanNa_V$ was detected in negative controls without the antibody (Figure 3Cc). The cells were also counterstained with Hoechst 33 258 to visualize nuclei (Figure 3Ca), and the double staining with this dye and $PanNa_V$ is shown in Figure 3Cd. Similarly, expression of Na_V proteins, by using anti-$Na_V1.6$ (Figure 5A), anti-$Na_V1.7$ (Figure 5B) and anti-$PanNa_V$ (Figure 5C) antibodies, was confirmed in PC cells. No expression of $PanNa_V$ was detected in negative controls without the antibody (Figure 5d). These results were consistent with the results of the RT-PCR studies.

Effect of siRNA for SCN8A and SCN9A on the expression of voltage-gated Na^+ channels

To inhibit the expression of SCN8A and SCN9A, we used siRNA methods. Transfection of siRNA conjugated with rhodamine was confirmed by fluorescent microscopy (Figure 4C). Two days after siRNA treatment, the inhibitory effect on the expression of SCN mRNA was analysed by real-time RT-PCR. The expression level of SCN8A and SCN9A mRNA in PC-3 cells was significantly inhibited by the corresponding siRNA, compared with non-silencing (negative control) siRNA, as shown in Figure 4D. The most effective inhibition of mRNA for SCN8A was with the SCN8A (86) structure (Figure 4D, $P < 0.001$, $n = 4$), and the most effective siRNA for SCN9A was SCN9A (91) (see Table 1 for structures; Figure 4D, $P < 0.001$, $n = 4$). As 48 h treatment was sufficient to reduce the expression level, we used the cells 48 h after the

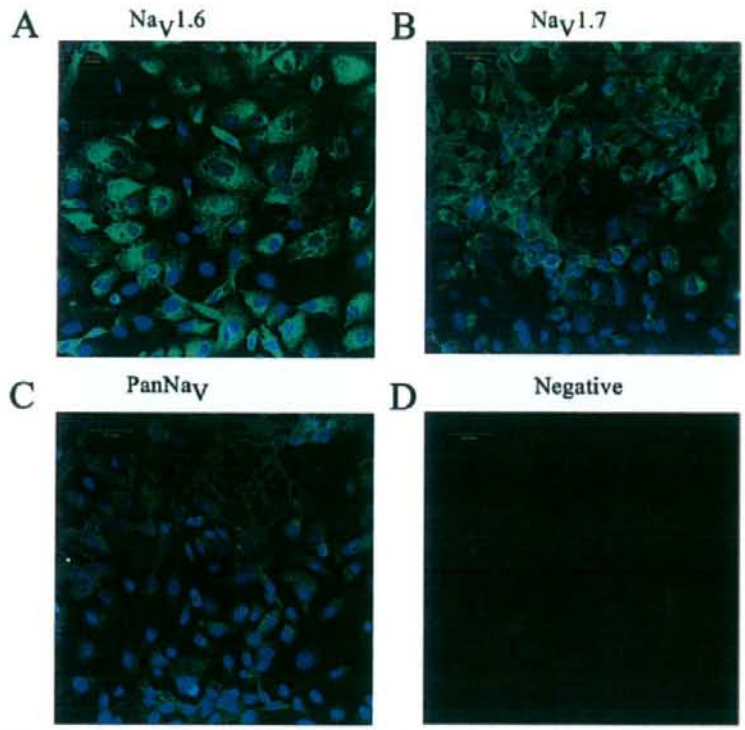

Figure 5 Immunocytochemical detection of $Na_V1.6$, $Na_V1.7$ and $PanNa_V$ in PC-3 cells. In A, double staining with Hoechst 33 258 and antibody to $Na_V1.6$. In B, staining with $Na_V1.7$ and in C with $PanNa_V$ antibodies is shown. Negative control (without antibody, D).

transfection to investigate the effect of siRNA for SCN8A (86) and SCN9A (91) in the subsequent experiments.

Effects of long-term treatment with EPA on fatty acid compositions of PC cells and mRNA levels of the Na^+ channel

Figure 6A shows the changes in fatty acid composition of phospholipids after treatment with EPA [C20:5 (ω-3)] for 2.7–72 h. The EPA, docosapentaenoic acid [DPA, C22:5 (ω-3)] and docosahexaenoic acid [DHA, C22:6 (ω-3)] content of the phospholipids increased in a time-dependent manner. On the other hand, arachidonic acid [AA, C20:4 (ω-6)] decreased time-dependently. Thus, the ratio of EPA to AA increased from 0.1 to 1.3 (24 h) and then 3.2 (72 h). The ratio of ω-3 to ω-6 also increased significantly.

Figure 6B shows the effects of 48 h treatment with EPA on the expression of SCN8A and 9A mRNA by real-time quantitative RT-PCR in PC-3 cells. The transcript levels were normalized to 18S ribosomal housekeeping gene. EPA (30 (M) was added to the cells before they reached confluence in culture medium supplemented with 7% FBS for 48 h. Treatment with EPA for 48 h significantly inhibited the expression of both SCN8A and SCN9A mRNA. Thus, these results suggested that longer exposures (48–72 h) to EPA decreased the level of the mRNA for Na channels carrying I_{Na}, after the EPA was incorporated into the cell lipids.

Effects of EPA on cell migration and proliferation

In order to determine the roles of Na^+ channels on cell migration and proliferation, PC-3 cells were treated with either TTX or siRNA. The cells transfected with siRNA for SCN9A (91) and/or SCN8A (86) were compared with the cells transfected with non-silencing (negative control) siRNA. TTX (10 μmol·L^{-1}, Figure 7A) significantly inhibited cell migration ($n = 6$, $P < 0.05$). In addition, siRNA for SCN9A inhibited cell migration ($n = 6$, $P < 0.05$), but a combination of siRNA for SCN8A and for SCN9A provided greater inhibition (Figure 7B). As shown in Figure 7C,D, EPA (30 μmol·L^{-1}) also significantly inhibited cell migration ($n = 6$, $P < 0.05$) in a similar way to TTX (10 μmol·L^{-1}).

Effects of TTX and the combination of siRNA targeted for SCN8A and SCN9A, on cell proliferation were investigated in PC-3 cells. Neither TTX (10 μmol·L^{-1}) nor siRNA had effect on cell proliferation at 24 and 48 h (Figure 8A,B, $n = 6$). However, EPA (30 μmol·L^{-1}) markedly inhibited cell proliferation, in contrast to TTX (Figure 8C).

Effects of EPA on endocytosis in PC-3 cells

Effects of TTX and siRNA targeted for both SCN8A and SCN9A on cell endocytosis were examined in PC-3 cells, by using HRP uptake. As shown in Figure 9A,B, TTX (1–10 μmol·L^{-1}, $n = 7$, Figure 9A) and the siRNA (Figure 9B) significantly

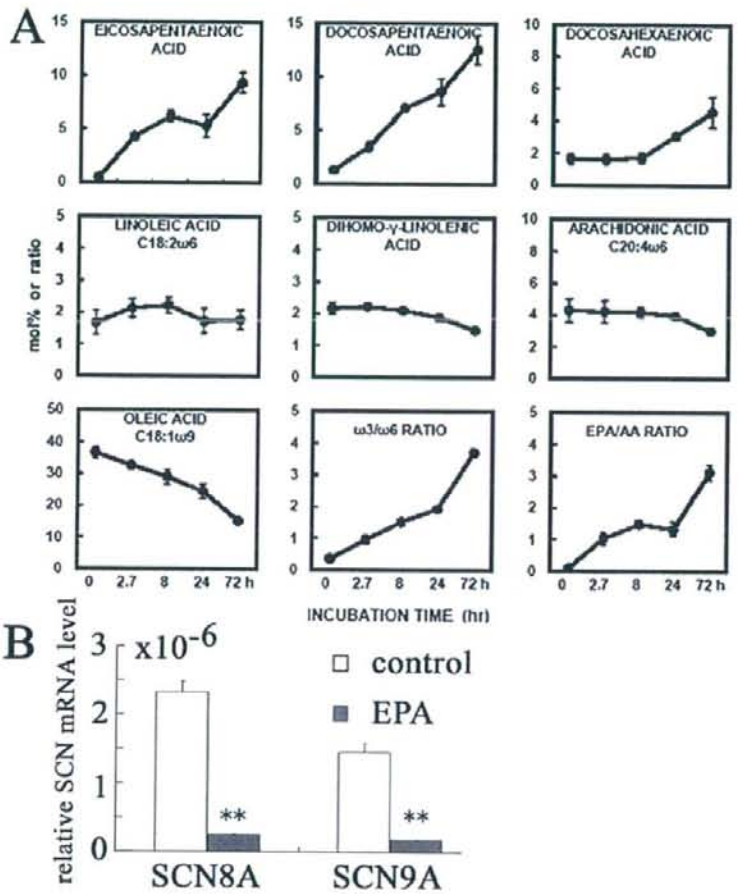

Figure 6 Effects of long-term exposure to EPA on fatty acid compositions of PC-3 cells and mRNA levels of the Na^+ channel proteins, in PC-3 cells. (A) Changes in fatty acid compositions of phospholipids in control cells and cells treated with EPA. The cells were treated with EPA (30 $\mu mol \cdot L^{-1}$) for 2.7–72 h. The changes of fatty acid composition in phospholipids (mol%) are indicated. The data represent means ± SEM value obtained from two different cells. (B) Effects of chronic treatment with EPA on the expression of SCN8A and 9A mRNA in PC-3 cells. SCN9A expression was assessed by real-time quantitative RT-PCR, and transcript levels were normalized to 18S ribosomal housekeeping gene. EPA (30 $\mu mol \cdot L^{-1}$) was added to the cells before they reached confluence in culture medium for 48 h. After incubation for 48 h in culture medium supplemented with 7% FBS, expression of mRNA for SCN8A and SCN9A in the presence of EPA was compared with that in the absence of EPA. $^{**}P < 0.01$ vs. control. EPA, eicosapentaenoic acid; FBS, fetal bovine serum; RT-PCR, reverse transcriptase polymerase chain reaction.

reduced HRP uptake into PC-3 cells ($P < 0.01$, $n = 7$), suggesting that I_{Na} is necessary for endocytosis in PC-3 cells. Also, EPA significantly inhibited HRP uptake into the cells in a concentration-dependent manner ($n = 7$; Figure 9C).

Discussion

The major findings of the present study were twofold. Firstly, EPA inhibited voltage-gated Na^+ current (I_{Na}) in prostate cancer cells via two independent mechanisms: by directly affecting the channel and rapidly inhibiting I_{Na} with an IC_{50} of approximately 6 $\mu mol \cdot L^{-1}$ or indirectly by decreasing the level of the mRNAs for channel proteins (SCA8A and SCN9A), carrying I_{Na}, after incorporation of EPA into cell lipids. Secondly, EPA, TTX and siRNA targeted for Na channel α-subunits inhibited metastatic functions (invasion and endocytosis) of the two cell lines. These results suggest that EPA could inhibit metastatic activity by blocking the up-regulated I_{Na} in prostate cancer cells. Such blockade may reduce the risk of prostate carcinoma and its progression, and consequently increase survival.

The present study shows the presence of I_{Na} in prostate cancer cells (Mat-LyLu rat prostate cancer cell lines and PC-3 human prostate cancer cell lines), which was consistent with previous papers (Grimes *et al.*, 1995; Fraser *et al.*, 2000; 2003; Anderson *et al.*, 2003; Bennett *et al.*, 2004; Krasowska *et al.*, 2004; Brackenbury and Djamgoz, 2006). TTX completely inhibited I_{Na} expressed in both cancer cell lines and, in Mat-LyLu cells, TTX had an IC_{50} value of approximately